Mathematical Modeling and Control of a Cost Effective AC Voltage Stabilizer

Hao Liu, Jihong Wang, *Senior Member, IEEE*, and Oleh Kiselychnyk, *Member, IEEE*

***Abstract*—AC voltage regulation is required in both the domestic and industrial sectors to avoid undesired effects from random voltage variations of the power supply. The paper introduces an ac voltage stabilizer/converter (ACVS) that is based on a controllable autotransformer technology. The proposed ACVS offers a specified strategy of voltage regulation, less harmonics, and low cost. The paper explains the operating principle of the ACVS and derives its nonlinear mathematical model. To ensure the desired performance of the ACVS while it is subject to uncertain input voltage and load variations, an optimal control strategy is designed. It is achieved via transforming the ACVS model extending with fictive axis emulation into a rotating reference frame and the linearization of the model via specific orientation of the reference frame and introducing a linear control action. Operation of the ACVS is simulated under different disturbances due to load and grid voltage changes, and compared to voltage stabilization with application of I and PI controllers. Experimental results are presented to demonstrate the voltage regulation technology.**

***Index Terms*—AC–AC power conversion, electric variables control, linear-quadratic control, power quality, voltage control.**

I. Introduction

UNSTABLE voltage and unexpected overrated voltage levels are common problems faced by both the domestic and commercial/industrial electricity users. This results in various power quality issues such as lighting dimming, loss of heat control, loss of optimal operation status, and loss of motor control [1]. These problems not only decrease the efficiency of the equipment operation but also lead to an unwanted extra electrical energy consumption. As for some more sensitive loads (for instance, personal computers, transceiver devices, and medical systems), the excessive high or low voltage of power supply may cause failure in operation and even harm the devices [2]. Although much effort has been made by the power suppliers in stabilizing the network voltage, voltage regulation may still be required at the consumer/demand side. It is reported that many approaches have been investigated and used in the compensation of voltage variations from the power supply [3].

Manuscript received August 13, 2015; revised November 19, 2015; accepted December 21, 2015. Date of publication January 01, 2016; date of current version June 24, 2016. This work was supported in part by the Research Grant EPSRC EP/L001004/1 from Engineering and Grant EP/J01043X/1 Physical Science Research Council, U.K., and the University of Warwick Ph.D. Scholarship. Recommended for publication by Associate Editor J. Acero.

H. Liu and O. Kiselychnyk are with the School of Engineering, University of Warwick, Coventry CV4 7AL, U.K. (e-mail: Hao.Liu@warwick.ac.uk; O.Kiselychnyk@warwick.ac.uk).

J. Wang is with the School of Engineering, University of Warwick, Coventry CV4 7AL, U.K. and also with Huazhong University of Science and Technology, Wuhan 430074, China. (e-mail: Jihong.Wang@warwick.ac.uk).

Color versions of one or more of the figures in this paper are available online at http://ieeexplore.ieee.org.

Digital Object Identifier 10.1109/TPEL.2015.2514180

Among those methods, a traditional transformer with power electronic controlled tap changers is reported recently [4]. The transformer is connected in between the power supply and the sensitive load. Part of the secondary winding is mounted with several taps and hence the whole winding is divided into a few sections. The tap changers are controlled by fast switches and designed to change the turn ratio of the transformer windings, in which the secondary voltage will vary to compensate the voltage sag/swell when necessary. This method has disadvantages which limits its applications. In fact, the adjustment of the voltage level is not smooth and has to be step changes; the range of voltage regulation is relatively narrow [5]; and the compensation by tap-changing transformer is accomplished with a time delay since the thyristor-based switches can be turned ON only once per ac cycle [3]. Hence, it is unlikely for this method to achieve fast and accurate voltage regulations.

With the advances of the high-speed power electronic switching devices, various topologies of power converters are proposed /developed to achieve controlled ac to ac conversion [6]–[8]. Bidirectional switches, which normally have two switching devices connected in series and each switch is paralleled with a diode for bypass, are adopted in the circuit for ac to ac conversion [9]. Adopting purely bidirectional switches and passive components, full range of ac voltage regulation can be achieved [10]–[12]. Since the full load current goes through the semiconductor switches in ac/ac converters, the power rating required for the switching devices needs to match the load power. So the cost for higher power rating converters will increase accordingly.

The paper presents a new ac/ac single-phase converter as an ac voltage stabilizer/converter (ACVS), in which the power electronic switching devices carry lower current due to integration of an autotransformer with an ac chopper, which, in turn, might reduce the cost of the converter. In this combination, the power electronic module is connected to the low-current primary winding side of the transformer and so the power rating to power electronic devices is significantly reduced [6]–[8]. Design of a voltage controller with such circuitry is challenging, mainly due to the nonlinear and discontinuous relationship within the system. A solution is proposed to address the challenge in this paper by transformation of the ACVS model into a two-phase representation in a rotating reference frame aligned with the output voltage vector. Through the mathematical derivation and theoretical analysis, the original ACVS model is converted into a linear model in the control and state space, in which the control task is to stabilize the output voltage.

A solution which resembles the proposed topology is reported in [13] for an ac single-phase dynamic voltage restorer. It is a combination of a transformer and a single-phase ac–ac matrix converter which not only regulates the voltage on the primary

winding but also allows the changing of its phase angle by 180°. A feed-forward control approach is used, improved by the internal control loop of the output voltage of the matrix converter. The control task for the mains voltage disturbance compensation is to track the desired sinusoidal reference voltage of the matrix converter dynamically, which requires initial synchronization of the control reference with the mains voltage. The requirement for tracking accuracy leads to the increased costs of the converter. A simpler feed-forward intuitive solution is presented in [14] where simplified static dependences are derived for the ac chopper duty ratio providing steady-state voltage stabilization without considering the ac chopper transients and possible variation of its and transformer parameters. Due to the nature of the feed-forward regulation (open loop control with disturbances compensation), it inevitably leads to steady-state voltage control errors. The ACVS circuit topology in the proposed paper has some similarities to the topology presented in [15], where an ac converter with a PID controller is designed for voltage sag protection not for full range of voltage stabilizer. Similar to [15], the voltage line conditioner in [16] is based on a PI feedback controller in which gains are tuned via an iterative simulation for the case of specific resistive load. This ad hoc approach possesses all disadvantages inherent to a nonlinear system controlled via single linear controller (I, PI, or PID): different control quality for different operating points; at the design stage, it is necessary to prove the stability of the control system and check the quality of control for all possible operating points; it frequently requires gains scheduling for solving the aforementioned problems. In the case presented in [16], different types of loads may also require different PI-controller gain values.

This paper develops a systematic voltage controller adopting a converter model-based approach, and rigorous design methods rooted from linear systems and the optimal control theory is applied to achieve predefined control quality. The approach proposed in this paper avoids sinusoidal reference tracking problem encountered in [13] and the drawbacks due to intuitive solutions reported in [14]–[16]. The main contributions of the paper present in the development of a whole ACVS dynamical mathematical model with systematically designed control and the improvement of the feedback control technology for single-phase voltage stabilizers that is different from the methods used in [13]–[16]. This paper gives a detailed description of the circuit topology and working principle of the ACVS. The mathematical model of the ACVS is developed and then transformed into a rotating reference frame aligned with the output voltage vector for simulation study and the optimal control development. The results of simulation and experiments are presented in Section V.

II. Description of the ACVS Circuit Topology and its Operation Principles

The circuit diagram of the proposed ACVS is shown in Fig. 1. It can be seen that the voltage stabilizer mainly consists of a transformer connected to form an autotransformer and four power electronic switches. The primary winding of the transformer is connected to the mains with the voltage $v_{\rm in}$ through a pair of pulse width modulation (PWM) controlled bidirectional

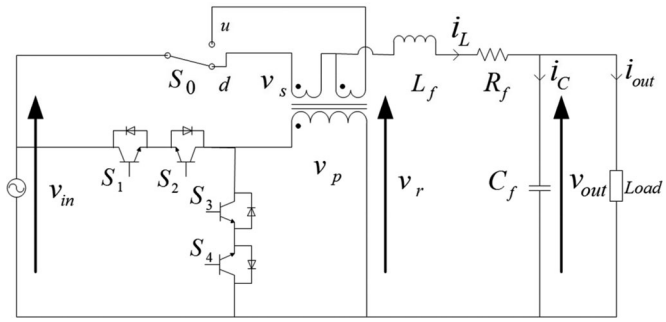

Fig. 1. Topology of the proposed ac voltage converter.

switches S_1-S_2. The switches S_3–S_4 are placed to provide a path for the primary winding energy dissipation to work with ON/OFF status changes of S_1–S_2. The "ON" and "OFF" status of the PWM control signal for the switches S_3–S_4 are complementary or opposite to the one applied to S_1–S_2. To avoid the overlapping of the two sets of switches, a delayed switching ON time is introduced. The transformer has two secondary windings which may have the same number of turns with polarity marks arranged as shown in Fig. 1 so the voltages of the two windings have an 180° phase shift. There is always only one of the secondary windings connected in series between the mains and the load through the relay switch S_0. Depending on the position of S_0, the secondary winding voltage will be added to (step-up mode) or subtracted from (step-down mode) the mains voltage to provide the load voltage. Change of the duty ratio of the PWM control is used to control the load voltage to the desired level. An *L–C* filter is used to smooth the output voltage.

A. Step-Down Mode

When the voltage $v_{\rm in}$ is higher than the reference voltage, this mode is applicable. In this mode, S_0 is switched to "d" position. The two pairs of switches S_1/S_2 and S_3/S_4 are switched ON and OFF with the PWM control. In the active state, S_1 and S_2 are conducting; both S_3 and S_4 are OFF. With S_1 and S_2 in ON status, the secondary winding voltage $v_{\rm in}/k$ is induced where k is the transformer winding ratio. The output voltage $v_{\rm out}$ is the difference between $v_{\rm in}$ and $v_{\rm in}/k$, excluding the drop of the voltage at the filter inductor. In freewheeling state, S_3 and S_4 are conducting; both S_1 and S_2 are OFF. The primary winding voltage of the transformer is zero so $v_{\rm out} = v_{\rm in}$ approximately in this state.

The PWM control gate signals for S_1–S_2 and S_3–S_4 are depicted in Fig. 2. The figure also shows the input voltage and the output voltage before filtering. The amplitude of the output voltage is regulated with the duty ratio changes. The higher the duty ratio is, the lower the output voltage will be.

B. Step-Up Mode

The step-up operation mode is designed for the case when the input voltage is below the required output voltage. In this mode S_0 is switched to "u" position. With the similar analysis conducted in the above section, the input and output voltages are shown in Fig. 3. The gate signals are the same as in Fig. 2.

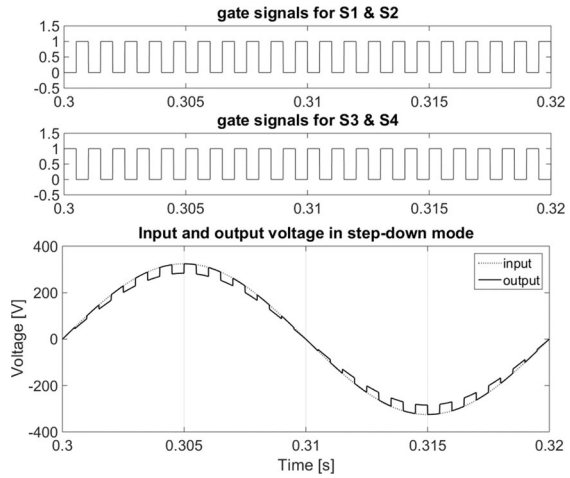

Fig. 2. Input and original output voltage without filtering comparison in step-down mode (duty ratio $D = 0.5$, switching frequency $f_s = 1$ kHz).

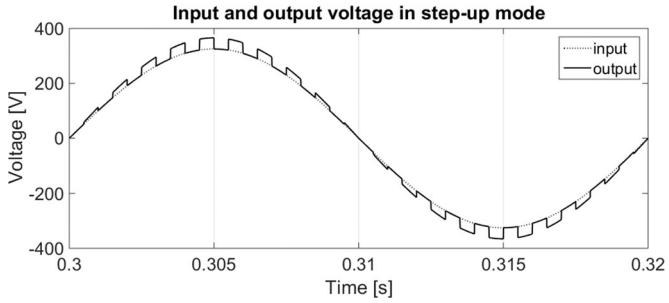

Fig. 3. Input and original output voltage without filtering comparison in step-up mode (duty ratio $D = 0.5$, switching frequency $f_s = 1$ kHz).

III. Modeling of the AC Voltage Stabilizer

A. Model of the ACVS

The voltage on the primary winding of the transformer is controlled by the four switches, which can be described by

$$v_p(t) = v_{\text{in}}(t)g(t) \tag{1}$$

where v_p is the primary winding voltage and g is the gate switching function of S_1–S_2.

The relationship between the primary winding voltage and the secondary winding voltage is expressed as

$$\frac{v_s(t)}{v_p(t)} = \pm\frac{1}{k} \tag{2}$$

where v_s is the transformer secondary winding voltage, and the upper sign is for the step-up mode, whereas the lower sign is for the step-down mode.

The voltage before the filter v_r is

$$v_r(t) = v_{\text{in}}(t) + v_s(t). \tag{3}$$

The output voltage accounts the voltage across the inductor of the *L–C* filter

$$v_{\text{out}}(t) = v_r(t) - L_f\frac{di_L(t)}{dt} - i_L(t)R_f \tag{4}$$

where i_L is the inductor current, L_f and R_f are the inductance and the resistance of the filter inductor, respectively. The inductor current is

$$i_L(t) = i_C(t) + i_{\text{out}}(t) = C_f\frac{dv_{\text{out}}(t)}{dt} + i_{\text{out}}(t) \tag{5}$$

where i_C is the capacitor current, C_f is the capacitance of the filter capacitor, and i_{out} is the load current.

Substituting (1)–(3) and (5) into (4) yields

$$v_{\text{out}}(t) = v_{\text{in}}(t)\left[1 \pm \frac{g(t)}{k}\right] - \left[L_fC_f\frac{d^2v_{\text{out}}(t)}{dt^2} + L_f\frac{di_{\text{out}}(t)}{dt} + R_fC_f\frac{dv_{\text{out}}(t)}{dt} + R_fi_{\text{out}}(t)\right]. \tag{6}$$

Assume that the duty ratio $D(t)$ is fixed in a single switching period. Then, the gate switching function $g$can be expressed as

$$g(t) = \begin{cases} 1 & nT_s < t < (n + D(t))T_s \\ 0 & (n + D(t))T_s < t < (n+1)T_s \end{cases} \tag{7}$$

where $n = 0, 1, 2, 3\ldots$ represents the number of sample time.

Applying Fourier series expansion to decompose (7), it can be obtained as follows [7]:

$$g(t) = D(t) + \sum_{m=1}^{\infty}\frac{2\sin(mD(t)\pi)}{m\pi}\cos(m\omega_s t) \tag{8}$$

where ω_s denotes the angular switching frequency.

According to (8), the switching function consists of the duty ratio and high-frequency harmonic components. Since the harmonics are filtered out by the *L–C* filter afterward, switching function $g(t)$can be replaced by $D(t)$approximately. Therefore, (6) can be rewritten as

$$v_{\text{out}}(t) = v_{\text{in}}(t)\left[1 \pm \frac{D(t)}{k}\right] - \left[L_fC_f\frac{d^2v_{\text{out}}(t)}{dt^2} + L_f\frac{di_{\text{out}}(t)}{dt} + R_fC_f\frac{dv_{\text{out}}(t)}{dt} + R_fi_{\text{out}}(t)\right]. \tag{9}$$

Equation (9) establishes the relationship between the input voltage, output voltage, and converter parameters with the load current as one of uncertain input variables, from which the following are noticed:

1) the output voltage is sinusoidal both in steady states and transients due to the input voltage being sinusoidal;
2) change of the magnitude of the input voltage v_{in} is a disturbance of the model;
3) another disturbance is the load current i_{out}which depends on the load type and it is unpredictable;
4) the control input is the duty ratio *D* which should be adjusted to keep the output voltage magnitude constant;
5) the control input is bounded between 0 and 1;
6) the model is nonlinear due to available sinusoidal input voltage and its product with the control action.

These features make the design of the output voltage magnitude controller a difficult task. However, a sufficient solution for low-cost implementation is found via nonstandard transformation of the model of the voltage converter.

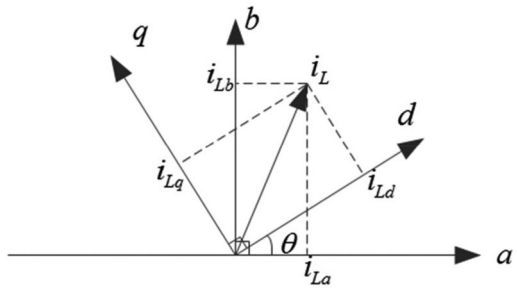

Fig. 4. Transformation of vectors from *a-b* to *d-q* reference frame.

B. Model Transformation

This section introduces a model transformation which converts the complex control design task of the sinusoidal ac voltage output magnitude into a linear control system design frame. The method is similar to the ac machines' two-phase description in an arbitrary rotating reference frame *d-q* instead of a stationary reference frame *a-b* [17]. A similar approach was adopted in [18] and applied to current loop control of a single-phase voltage-source converter, named fictive-axis emulation.

It is assumed that a fictive converter runs in parallel along with the actual one with all sinusoidal signals shifted in 90 electrical degrees. Both converters have the same parameters. Further, all the variables of the actual converter are marked with the subscripts by index "a" whereas all the variables of the fictive one are marked by index "b." As a result, there is a two-phase fictive converter generalized.

Then, (5) for the two-phase converter can be put into a vector form

$$\mathbf{i_{Lab}}(t) = C_f \frac{d\mathbf{v_{outab}}(t)}{dt} + \mathbf{i_{outab}}(t) \tag{10}$$

where $\mathbf{i_{Lab}}(t) = [\, i_{La} \;\; i_{Lb}]^{\,T}$, $\mathbf{v_{outab}}(t) = [\, v_{\mathrm{out}a} \;\; v_{\mathrm{out}b}]^{\,T}$, and $\mathbf{i_{outab}}(t) = [\, i_{\mathrm{out}a} \;\; i_{\mathrm{out}b}]^{\,T}$.

Equation (4) with substitutions of (1)–(3) and accounting (8) is transformed to

$$\mathbf{v_{outab}}(t) = \mathbf{v_{inab}}(t)\left[1 \pm \frac{D(t)}{k}\right] - L_f \frac{d\mathbf{i_{Lab}}(t)}{dt} - \mathbf{i_{Lab}}(t)R_f \tag{11}$$

where $\mathbf{v_{inab}}(t) = [\, v_{\mathrm{in}a} \;\; v_{\mathrm{in}b}]^{\,T}$. Note that $D(t)$ is a scalar function and it is the control input for both "a" and "b" axes. The control splits into two elements of the vector below

$$\mathbf{v_{pab}}(t) = \mathbf{v_{inab}}(t)D(t) \tag{12}$$

where $\mathbf{v_{pab}}(t) = [\, v_{pa} \;\; v_{pb}]^{\,T}$, and $\mathbf{v_{pa}}, \mathbf{v_{pb}}$ denote the primary winding voltages in the real and fictive converters, respectively.

A *d-q* orthogonal reference frame is introduced which is rotating with the velocity equal to the angular frequency ω of v_{out}. The angle between the *d-q* and *a-b* frames is θ and $d\theta/dt = \omega$. Any vector in the stationary *a-b* reference frame can be transformed to the *d-q* frame through rotating it by angle θ in the direction opposite to the direction of rotation of the *d-q* frame. Fig. 4 shows an example of transformation for the inductor current vector.

Mathematically, the transformation is described as

$$\begin{bmatrix} i_{Ld} \\ i_{Lq} \end{bmatrix} = \begin{bmatrix} \cos\theta & \sin\theta \\ -\sin\theta & \cos\theta \end{bmatrix} \begin{bmatrix} i_{La} \\ i_{Lb} \end{bmatrix}. \tag{13}$$

A similar transformation applies for the rest of the vectors. In result, the elements of the vectors in the *d-q* frame are constants in steady states and not sinusoidal during transients, although the elements of the corresponding vectors in the *a-b* frame are sinusoidal.

Equations (10) and (11) in the *d-q* reference frame are obtained as

$$\mathbf{i_{Ldq}}(t) = C_f \frac{d\mathbf{v_{outdq}}(t)}{dt} + C_f \omega \mathbf{J} \mathbf{v_{outdq}} + \mathbf{i_{outdq}}(t) \tag{14}$$

$$\mathbf{v_{outdq}}(t) = \mathbf{v_{indq}}(\mathbf{t})\left[1 \pm \frac{D(t)}{k}\right] - L_f \frac{d\mathbf{i_{Ldq}}(t)}{dt} - L_f \omega \mathbf{J} \mathbf{i_{Ldq}}(t) - \mathbf{i_{Ldq}}(t)R_f \tag{15}$$

where $\mathbf{v_{outdq}}(t) = [v_{\mathrm{out}d} \;\; v_{\mathrm{out}q}]^T$, $\mathbf{i_{outdq}}(t) = [i_{\mathrm{out}d} \;\; i_{\mathrm{out}q}]^T$, $\mathbf{i_{Ldq}}(t) = [i_{Ld} \;\; i_{Lq}]^T$, $\mathbf{v_{indq}}(t) = [v_{\mathrm{in}d} \;\; v_{\mathrm{in}q}]^T$, and $\mathbf{J} = \begin{bmatrix} 0 & -1 \\ 1 & 0 \end{bmatrix}$.

It is noticed that additional terms (due to available time derivatives) depending on ω are introduced into the equations via the transformation. The corresponding equations for *d*- and *q*-axes are coupled in (14) and (15) due to $\mathbf{J}$ whereas the initial equations for *a* and *b*-axes in (10) and (11) are independent.

The system of (14) and (15) can be organized in a state-space form as follows:

$$\dot{\mathbf{X}} = \mathbf{A}\mathbf{X} + \mathbf{B}u + \mathbf{W} \tag{16}$$

where $\mathbf{X} = [\, v_{\mathrm{out}d} \quad v_{\mathrm{out}q} \quad i_{Ld} \quad i_{Lq} \,]^T$, $u = D(t)$,

$$\mathbf{A} = \begin{bmatrix} 0 & \omega & 1/C_f & 0 \\ -\omega & 0 & 0 & 1/C_f \\ -1/L_f & 0 & -R_f/L_f & \omega \\ 0 & -1/L_f & -\omega & -R_f/L_f \end{bmatrix}$$

$$\mathbf{B} = \begin{bmatrix} 0 \\ 0 \\ \dfrac{\pm v_{\mathrm{in}d}}{kL_f} \\ \dfrac{\pm v_{\mathrm{in}q}}{kL_f} \end{bmatrix}, \quad \mathbf{W} = \begin{bmatrix} \dfrac{-1}{C_f} & 0 \\ 0 & \dfrac{-1}{C_f} \\ 0 & 0 \\ 0 & 0 \end{bmatrix} \begin{bmatrix} i_{\mathrm{out}d} \\ i_{\mathrm{out}q} \end{bmatrix} + \begin{bmatrix} 0 & 0 \\ 0 & 0 \\ \dfrac{1}{L_f} & 0 \\ 0 & \dfrac{1}{L_f} \end{bmatrix} \begin{bmatrix} v_{\mathrm{in}d} \\ v_{\mathrm{in}q} \end{bmatrix}.$$

Align the *d-q* reference frame with the output voltage vector. Then,

$$v_{\text{out}d} = |v_{\text{out}dq}| = |v_{\text{out}ab}| = |v_{\text{out}}|, v_{\text{out}q} = 0, \dot{v}_{\text{out}q} = 0 \tag{17}$$

where $|v_{\text{out}}|$ is the magnitude of the actual single-phase output voltage. Note that the magnitude of any vectors in the *d-q* and *a-b* reference frames is same.

The approach from [18] introduces a decoupling control making the d and q-axes equations independent. Inspired by the methodology, the paper proposes a new solution which is less complicated in control implementation and it is feasible in this case due to specific topology of the voltage stabilizer.

The second equation of (16) in the reference frame aligned with the output voltage vector gives the following algebraic equation for relating i_{Lq} to output voltage and current:

$$i_{Lq} = C_f \omega |v_{\text{out}}| + i_{\text{out}q} \tag{18}$$

.

From (18), i_{Lq} is not an independent variable so it can be eliminated from the third equation of (16). Then, the fourth equation of (16) gives dynamics of $v_{\text{in}q}$

$$v_{\text{in}q} = \frac{kL_f}{k \pm D(t)} \left[2\omega i_{Ld} + \frac{R_f C_f \omega}{L_f} |V_{\text{out}}| + \frac{R_f}{L_f} i_{\text{out}q} - \omega i_{\text{out}d} + \frac{d i_{\text{out}q}}{dt} \right]. \tag{19}$$

Note that even if $|v_{\text{in}}|$ is a constant, its components $v_{\text{in}q}$ and $v_{\text{in}d} = \sqrt{|v_{\text{in}}|^2 - v_{\text{in}q}^2}$ vary during control, meaning that the angle of the input voltage vector changes with respect to the angle of the output voltage vector.

The parameters of the filter are chosen in such a way to provide a negligible angle difference between the input and output voltage vectors of the ACVS, which results in $v_{\text{in}q} \approx 0$. Therefore, from control design point of view, it is possible to assume $v_{\text{in}d} = |v_{\text{in}}|$ and consider the small deviation $|v_{\text{in}}| - v_{\text{in}d}$ as an additional external disturbance of the magnitude of the input voltage. Due to this, model (16) can be reduced to the second order with the state vector $\mathbf{X}_1 = [\, |v_{\text{out}}| \; i_{Ld} \,]^T$

$$\dot{\mathbf{X}}_1 = \mathbf{A}_1 \mathbf{X}_1 + \mathbf{B}_1 u + \mathbf{W}_1 \tag{20}$$

where

$$\mathbf{A}_1 = \begin{bmatrix} 0 & 1/C_f \\ C_f\omega^2 - 1/L_f & -R_f/L_f \end{bmatrix}$$

$$\mathbf{B}_1 = \begin{bmatrix} 0 \\ \pm |v_{\text{in}}| / (kL_f) \end{bmatrix}$$

$$\mathbf{W}_1 = \begin{bmatrix} -1/C_f & 0 \\ 0 & \omega \end{bmatrix} \begin{bmatrix} i_{\text{out}d}(t) \\ i_{\text{out}q}(t) \end{bmatrix} + \begin{bmatrix} 0 \\ 1/L_f \end{bmatrix} |v_{\text{in}}|.$$

The order of the model is reduced by 2 and it has the following features:

1) the output of the model is the output voltage magnitude which is the same in both *d-q* and *a-b* reference frames;
2) the control input is present only in one equation of the model and it is the same in both *d-q* and *a-b* reference frames;
3) the disturbances of the model are the load currents and the input voltage magnitude;
4) the model is still nonlinear due to the product $|v_{\text{in}}|u$.

IV. Control Strategy

The goal of the control is to adjust automatically the duty ratio to stabilize the output voltage magnitude (or rms value) at the rated value $|v_{\text{out}}|^*$ in the presence of disturbances due to changes of the magnitude of the mains voltage and the voltage variations on the filter as the result of the load change.

Model (20) can be easily linearized in the vicinity of an operating point allowing straightforward application of modern and classic control methodologies to design the voltage controller in the *d-q* reference frame. The paper proposes an alternative approach introducing a new control input $u_2 = |v_{\text{in}}| D(t)$ which makes the model linear. Various robust control strategies can be applied, such as, PID control and robust deterministic control [19]. In this paper, a robust linear-quadratic regulator (LQR) for voltage control is considered. Note that$|v_{\text{in}}|$varies within a relatively small range and its variation is much slower compared with the control action.

To obtain a zero steady-state control error, model (20) is augmented with an additional state coordinate as an integral of the voltage magnitude error and the corresponding equation

$$v_i = \int_0^t (|v_{\text{out}}| - |v_{\text{out}}|^*) dt \tag{21}$$

.

Combining (20) and (21) with accounting $u_2 = |v_{\text{in}}| D(t)$, the state-space model is transformed to

$$\dot{\mathbf{X}}_2 = \mathbf{A}_2 \mathbf{X}_2 + \mathbf{B}_2 \mathbf{u}_2 + \mathbf{W}_2 \tag{22}$$

where

$$\mathbf{X}_2 = \left[\, |v_{\text{out}}| \; i_{Ld} \; v_i \,\right]^T, \mathbf{u}_2 = u_2$$

$$\mathbf{A}_2 = \begin{bmatrix} 0 & 1/C_f & 0 \\ C_f\omega^2 - 1/L_f & -R_f/L_f & 0 \\ 1 & 0 & 0 \end{bmatrix}$$

$$\mathbf{B}_2 = \begin{bmatrix} 0 \\ \pm 1/(kL_f) \\ 0 \end{bmatrix}, \quad \mathbf{W}_2 = \begin{bmatrix} -i_{\text{out}d}/C_f \\ \omega i_{\text{out}q} + |v_{\text{in}}| / L_f \\ -|v_{\text{out}}|^* \end{bmatrix}.$$

The quadratic cost function for system (22) is defined [19]

$$J = \int_0^\infty (\mathbf{X}_2^T \mathbf{Q} \mathbf{X}_2 + \mathbf{u}_2^T \mathbf{R} \mathbf{u}_2) dt \tag{23}$$

where $\mathbf{Q}$ and $\mathbf{R}$ are the matrices of positive symmetric weighting, expressed as diagonal matrices. The optimal control law with integral feedback is expressed as [20]–[22]

$$u_2 = -\mathbf{K} \mathbf{X}_2 \tag{24}$$

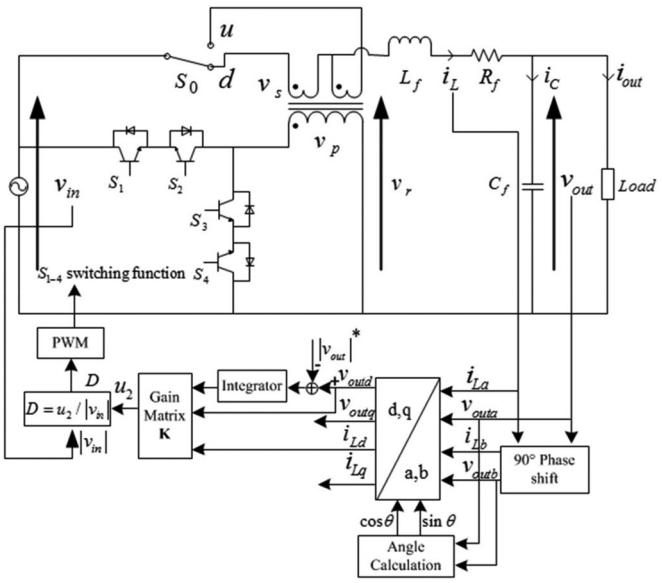

Fig. 5. Block diagram of the proposed single-phase ACVS with *d-q* transformation and LQR control.

where the gain matrix $\mathbf{K} = \mathbf{R}^{-1}\mathbf{B}_2^T\mathbf{P}$ is obtained by solving the Riccati equation

$$\mathbf{P}\mathbf{A}_2 + \mathbf{A}_2^T\mathbf{P} - \mathbf{P}\mathbf{B}_2\mathbf{R}^{-1}\mathbf{B}_2^T\mathbf{P} + \mathbf{Q} = \mathbf{0} \tag{25}$$

.

Note that LQR feedback gains for the step-up and step-down modes will be the same only with opposite signs. Due to this, the sign before reference in (21) depends on the operation mode, meaning that for the output voltage increase the duty ratio is increased in the step-up mode and it is reduced in the step-down mode.

The required for control duty ratio can be computed as

$$D(t) = u_2 / |v_{\text{in}}| \tag{26}$$

.

The block diagram of the proposed single-phase ACVS with *d-q* transformation and LQR control is depicted in Fig. 5. The angle of the *d-q* reference frame is computed via $\cos\theta = v_{\text{out}a}/|v_{\text{out}ab}|$ and $\sin\theta = v_{\text{out}b}/|v_{\text{out}ab}|$.

V. Simulation and Experimental Study

To verify the previous analyses, the mathematical model of the proposed ACVS and its *d-q* transformation are established in MATLAB/Simulink. The values of parameters are listed in Table I. To start with, the open loop system is set up to investigate the equivalence of the original model according to (16) and simplified model based on (20) in the *d-q* reference frame. Next, the closed loop system with proposed LQR feedback control illustrated in Fig. 5 is built and simulated while it is connected with different types of loads. The simulation results are compared with the results when PI and I controllers are used to evaluate the performance of the proposed LQR control.

The LQR gain matrix $\mathbf{K} = [-3.62 \times 10^{-5} \ -0.0028 \ -7.07]$ was obtained using MATLAB control design tool "LQR" for the step-down mode and $\mathbf{Q} = \text{diag}\{0.25\ 0.25\ 25\}, \mathbf{R} = [1]$, which were chosen iteratively to provide better dynamic performance.

TABLE I
Circuit Parameters

Parameter	Name	Value	Unit
Turn Ratio	k	8	–
Filter capacitance	C_f	1	μF
Filter inductance	L_f	3.9	mH
Filter resistance	R_f	0.1	Ω
Voltage frequency	f	50	Hz
Switching frequency	f_s	20	kHz
Referred output voltage magnitude (rms value)	$\lvert V_{\text{out}}\rvert^*$	310.2 (220)	V
Input voltage magnitude (rms value)	$\lvert V_{\text{in}}\rvert$	310.2±10% (220±10%)	V
Load current rms value	I_{out}	0–10	A

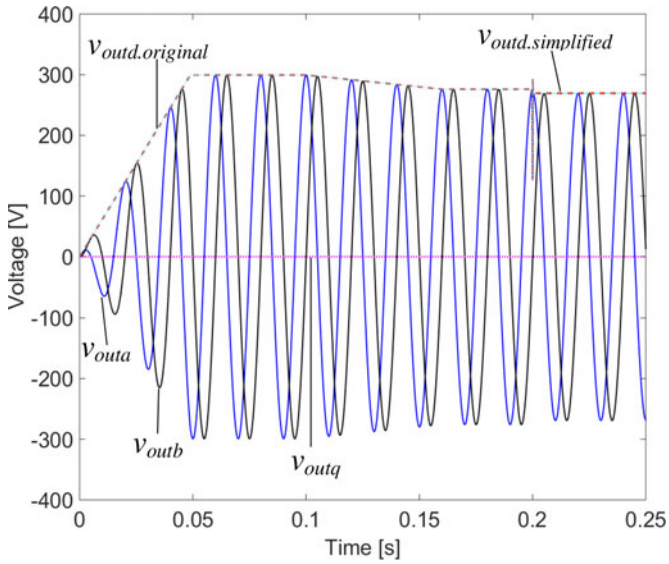

Fig. 6. Output voltages in the *a-b* and *d-q* reference frames.

A. Simulation Results of d-q Transformation

Comparison of the simulation results of the ACVS (without control) model (10), (11) in the *a-b* reference frame with model (16) in the *d-q* reference frame aligned with the output voltage vector according to (17)–(19), and with reduced order model (20) is shown in Figs. 6 and 7 for the step-down mode. The state variables of model (16) are marked with subscripts "original" and the variables of model (20) are denoted with subscripts "simplified." From 0 to 0.05 s, the responses of the models to linear increase of the magnitude of the input voltage from 0 up to its rated value are simulated for the case of no load and constant duty ratio value of 0.3. The reached steady state is kept till 0.1 s. After that, the duty ratio is increased linearly from 0.3 to 0.9 at t = 0.15 s causing the voltage amplitude reduction. At t = 0.2 s, there is a step change of resistive load current from 0 to 9.5 A leading to the voltage magnitude drop. Note that as expected $v_{\text{out}q} = 0$ and $v_{\text{out}d.\text{original}} = |v_{\text{out}ab}|$ for all times.

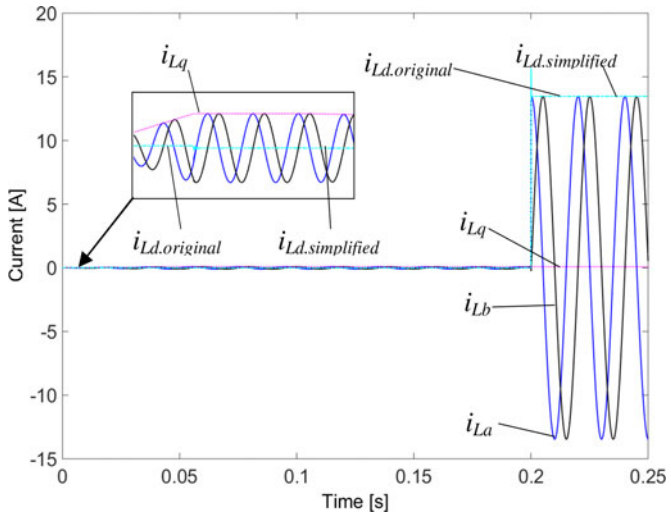

Fig. 7. Inductor currents in the *a-b* and *d-q* reference frames.

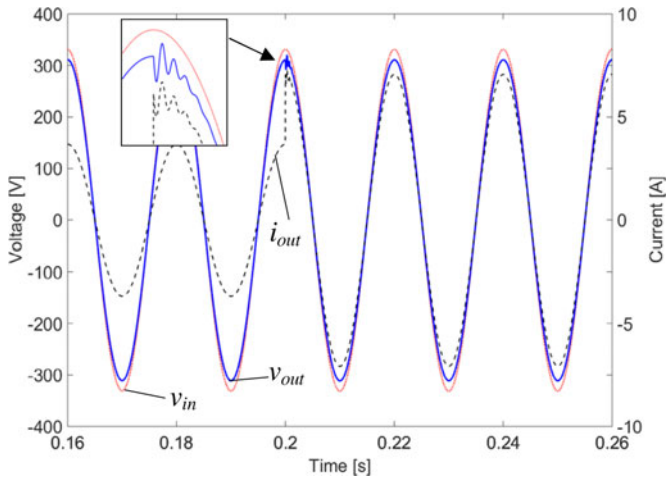

Fig. 8. Voltages and current instantaneous values with step changed resistive load.

The difference between $v_{\mathrm{out}d.\mathrm{original}}$ and $v_{\mathrm{out}d.\mathrm{simplified}}$ is tiny (not exceeding 0.01%).

Note that in steady state the first equation of model (16) gives $i_{Ld} = i_{\mathrm{out}d}$ in the reference frame aligned with the output voltage vector. Thus, for the steady state with no load $i_{Ld} = 0$ while $i_{Lq} \neq 0$ explained by (18) as shown in the subplot of Fig. 7. The difference between $i_{Ld.\mathrm{original}}$ and $i_{Ld.\mathrm{simplified}}$ is also negligible (not bigger than 0.01%) validating the reduced order model for the control design purpose.

B. Simulation Results of Voltage Control With Different Loads

Extensive simulation studies were performed for the system with the LQR controller depicted in Fig. 5 for the step-down mode. The results for instantaneous input and output voltages, and load currents are shown in Figs. 8, 10, and 12. Theyare also compared to the results obtained for the system when the LQR controller is replaced by I or PI controllers with rms output voltage feedback instead of the voltage magnitude (see Figs.

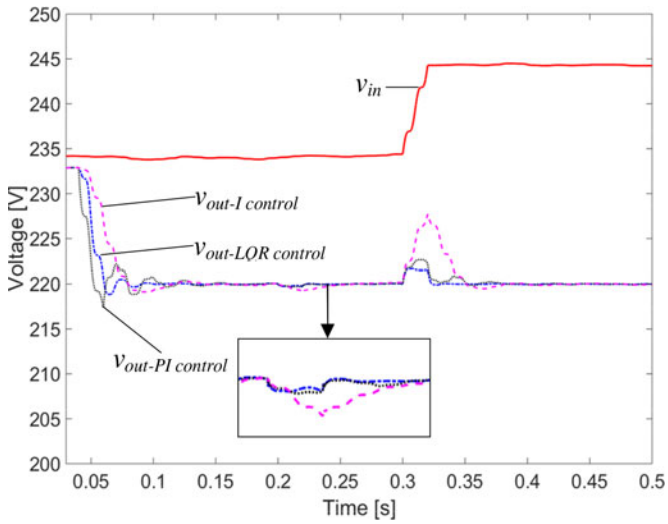

Fig. 9. Voltage rms values with step changed resistive load and input voltage increase.

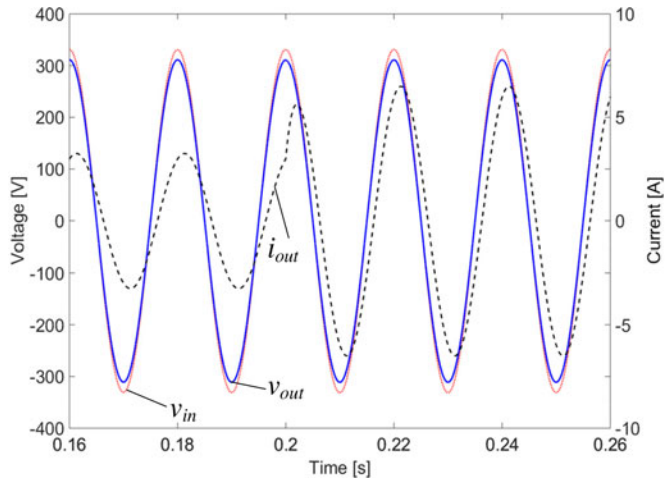

Fig. 10. Voltages and current instantaneous values with step changed inductive load.

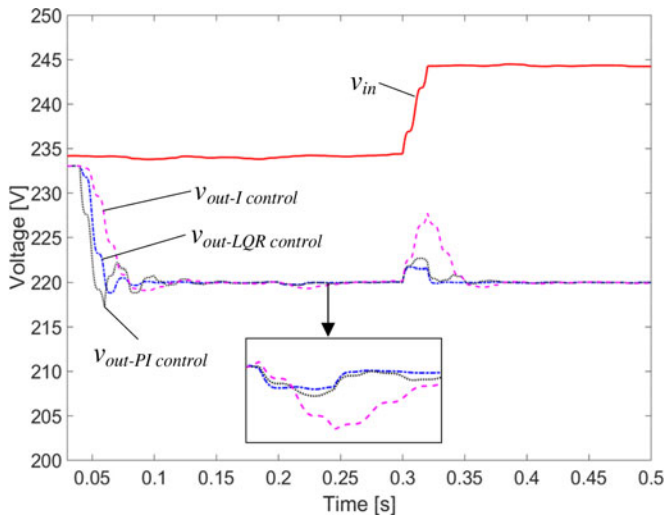

Fig. 11. Voltage and current rms values with step changed inductive load and input voltage increase.

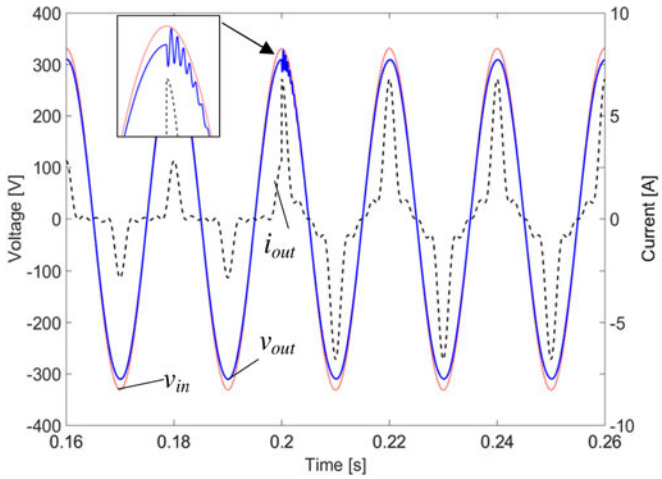

Fig. 12. Voltages and current instantaneous values with step changed nonlinear load.

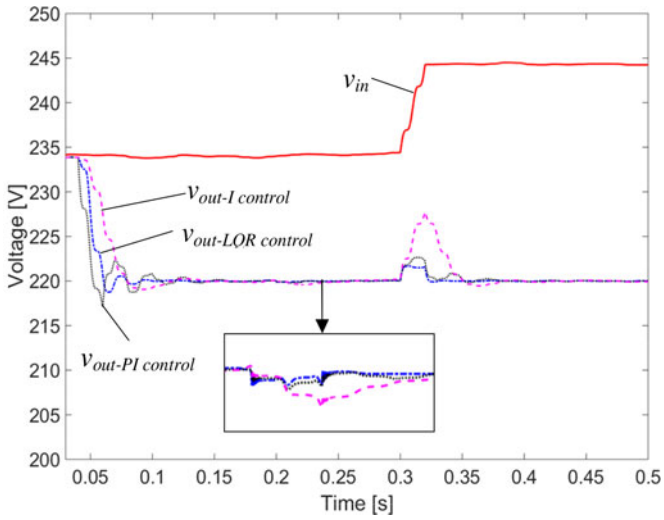

Fig. 13. Voltage and current rms values with step changed nonlinear load and input voltage increase.

9, 11 and 13), and without *d-q* transformation and (26). For the convenience of the comparison, the corresponding figures show rms values computed for each moment of time instead of the magnitudes. The parameters of I and PI controllers were chosen iteratively to provide the best possible performance of the system.

During the simulations all controllers were engaged from 0.04 s to start the control from a nonzero steady state and to allow initial computation of the output voltage rms value for two periods. In all cases, the initial operation of the controllers reducing the output voltage rms value from its initial value to the referred value is researched. Then, restoring the output voltage after step change of the corresponding load at 0.2 s is investigated. Finally, the responses of the controllers to the increase of the magnitude of the input voltage after 0.3 s are simulated.

1) Operation With Resistive Load: Fig. 8 shows that the distortion of the sinusoidal shape of the output voltage lasts for less than one-eighth of the period. After the engagement of the controllers (see Fig. 9), the output voltage rms values are gradually reduced to the reference value as 220 V. The proposed LQR controller demonstrates the shortest settling time. After the load current increase at 0.2 s, the response overshoot of the system with I controller is much higher than in the cases of two other controllers. For the input voltage 10-V-rms quick increase, the LQR controller also leads to the best performance in terms of response time and overshoot.

2) Operation With Inductive Load: Fig. 10 shows that the distortions of the sinusoidal shape of the output voltage are less and shorter in this case than for the resistive load. As expected, there is a phase difference between the output voltage and current while the output voltage is still in phase with the input voltage. When the inductive load increases from 2.3 to 4.6 A at 0.2 s, the voltage starts to drop slightly and then restores to the reference value with settling time 0.1 s, which is illustrated in the zoom-in view of Fig. 11. Fig. 11 also shows that the proposed LQR controller provides lower voltage overshoot and shorter settling time for both load and input voltage changes compared with PI and I controllers.

3) Operation With Nonlinear Load: Although the load current is highly distorted, the output voltage (see Fig. 12) has a low harmonic distortion with 0.26% THD priory to the step load change at 0.2 s. After the current rises up, the THD increases to 1.64% and is still within the 5% limit of the standard IEEE 519/92. The simulation results in Fig. 13demonstrate that the LQR controller gives the best performance among three controllers in terms of the settling time and overshoot.

C. Experimental Results

A prototype of ACVS with the proposed topology was implemented and tested, based on ST7FLITE35F2M6 microcontroller with embedded four channel PWM generator and seven multiplexed channel 10-bit analogue to digital converter. Parameters of its main components are shown in Table I. The bidirectional switches are formed by two HGTG5N120BND insulated gate bipolar transistors (IGBTs) from Fairchild. Each pair of the two IGBTs (21 A, 1200 V) is connected in emitter to emitter configuration. The input voltage, output voltage, and current are measured via National Instruments data acquisition system NI PXIe-6358. The chopped voltage on the primary winding of the transformer is observed via an oscilloscope at 100 MHz.

During experiments the grid voltage did not experience significant and fast changes. However, it oscillated slowly around or drifted away slowly from some steady-state value. It allowed the implementation of the controller with proportionally reduced gains in matrix $\mathbf{K}$, which provided less influence of the controller response to the voltage fluctuations on the steady-state output voltage value.

Fig. 14 illustrates the chopped voltage measured on the primary winding. The voltage is equal to either the input voltage in active state or is close to zero in freewheeling state, which is due to the nonzero turn-on resistance of IGBTs.

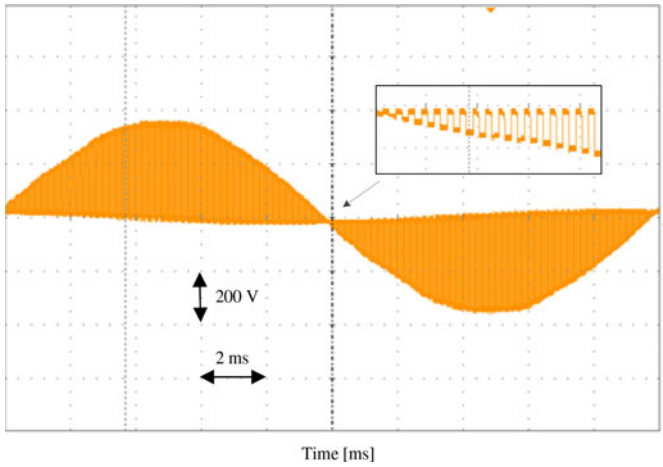

Fig. 14. Measured chopped voltage on the primary winding of the transformer.

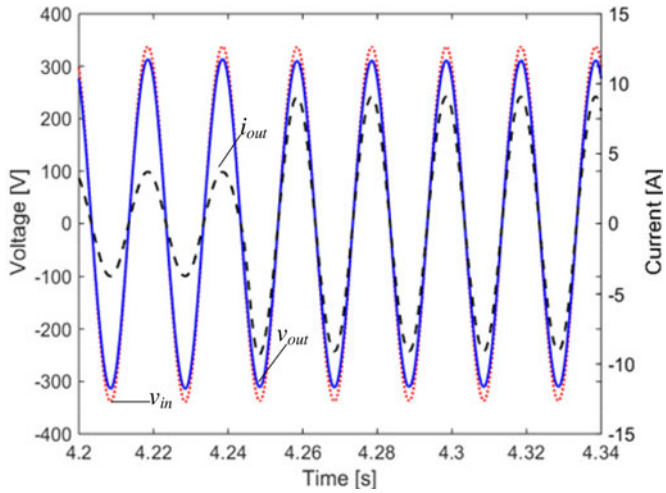

Fig. 15. Experimental results of instantaneous input voltage, output voltage, and output current.

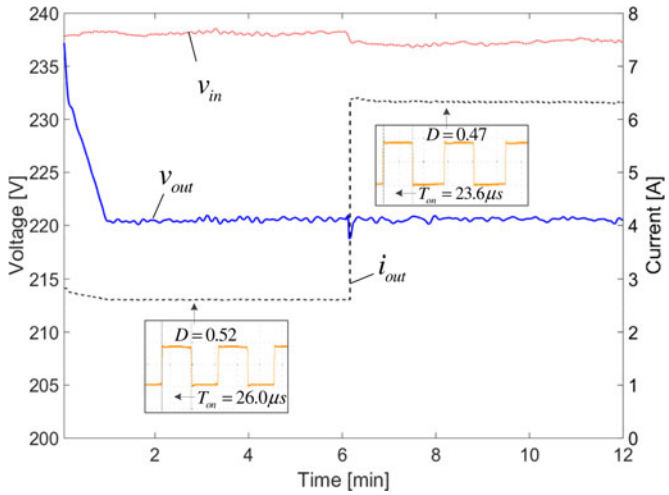

Fig. 16. Experimental results of input voltage, output voltage, and current rms values.

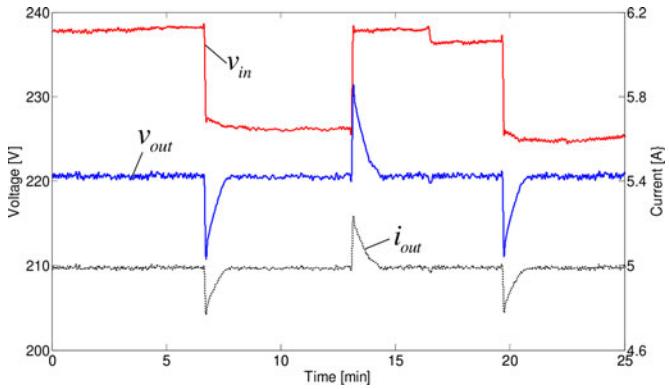

Fig. 17. Experimental results of input voltage, output voltage, and current (rms values) subject to mains voltage disturbances.

The measured instantaneous input voltage, output voltage, and output current are shown in Fig. 15 for the case of the resistive load step change. The output voltage demonstrates a good sinusoidal waveform in phase with the input voltage with slightly reduced amplitude. The temporary voltage drop caused by the load increase was less than 2 V.

Fig. 16 shows the rms values of input voltage, output voltage, and current for a longer experiment. It can be observed that the input voltage fluctuates slightly over time while the output voltage is always controlled to remain at the reference voltage during the test. The output voltage is close to the input voltage before the ACVS is engaged. When the controller starts to operate, the output voltage keeps reducing for a while and then reaches to 220V with a duty ratio 0.52 as shown in zoomed area of Fig. 16. To accelerate the process, the controller uses two different sets of gains depending on the difference between the input and output voltages. After a step resistive load change occurs, the output voltage drops instantly and then restores to 220V with the action of ACVS. Note that the load increase causes the input voltage decrease due to the nonideal grid. After transients, the duty ratio is set to 0.47 to maintain the output voltage at the referred level.

Fig. 17 demonstrates the behavior of the ACVS subject to input voltage disturbances introduced via input voltage regulation, for a specific resistive load. The parameters of the controller are the same as those used in the experimental results shown in Fig. 16. In Fig. 17, initially, the controller maintains the stable output voltage in the presence of the slow and small mains voltage drifting disturbances (input voltage is equal to the mains voltage). Then, the input voltage is reduced by 11 V. The output voltage decreases instantaneously and is smoothly restored by the controller to the reference value. Further the case of the input voltage with an 11 V increase is investigated. The controller restores smoothly the disturbed output voltage to its referred value. Next a slow drifting drop of the mains voltage (around 2 V) happens and the maximum transient output voltage deviation does not exceed 1 V. At the end, the test with the input voltage decrease is repeated. The performance of the controller is maintained from the responses of the measured voltage and current output shown in Fig. 17. Proportionally increased gains in matrix $\mathbf{K}$ of the LQR controller provide faster voltage transients with the similar curve shapes.

VI. Conclusion

The paper introduces an ac voltage stabilizer which has a lower cost compared with a full-range ac/ac converter. The working principle and the main characteristics of the ACVS are discussed. The mathematical model of the ACVS is developed and transformed into a *d-q* rotating reference frame to obtain a simplified model for the convenience of analysis. The simulation study convinces that the full ACVS model and the simplified *d-q* frame model give the agreed responses, and performance of the *d-q* frame model provides a useful platform for the development and analysis of new robust controls to the ACVS for both the academic and industrial communities. The initial study on control strategies is encouraging for performance improvement with disturbances from both supply voltage and the load variations. The experimental results demonstrates how the ACVS works and behaves in a real-life environment.

References

[1] A. Felce, G. Matas, and Y. Da Silva, "Voltage sag analysis and solution for an industrial plant with embedded induction motors," in *Proc. IEEE 39th Ind. Appl. Soc. Meet./Ind. Appl. Conf.*, 2004, vol. 4, pp. 2573–2578.

[2] S. Z. Djokic, J. Desmet, G. Vanalme, J. V. Milanovic, and K. Stockman, "Sensitivity of personal computers to voltage sags and short interruptions," *IEEE Trans. Power Del.*, vol. 20, no. 1, pp. 375–383, Jan. 2005.

[3] A. Sannino, M. G. Miller, and M. H. J. Bollen, "Overview of voltage sag mitigation," in *Proc. Power Eng. Soc. Winter Meet.*, 2000, vol. 4, pp. 2872–2878.

[4] S. M. Bashi, "Microcontroller-based fast on-load semiconductor tap changer for small power transformer," *J. Appl. Sci.*, vol. 5, no. 6, pp. 999–1003, 2005.

[5] N. Yorino, M. Danyoshi, and M. Kitagawa, "Interaction among multiple controls in tap change under load transformers," *IEEE Trans. Power Syst.*, vol. 12, no. 1, pp. 430–436, Feb. 1997.

[6] Z. Jie, Z. Yunping, Y. Weifu, L. Lei, and L. Fen, "Research on AC chopper power module with module parallel control," in *Proc. IEEE Appl. Power Electron. Conf. Expo.*, 2008, pp. 1324–1327.

[7] B.-H. Kwon, B. D. Min, and J. H. Kim, "Novel topologies of AC choppers," *IEE Proc. Electr. Power Appl.*, vol. 143, no. 4, pp. 323–330, 1996.

[8] J. H. Kim, B. D. Min, B. H. Kwon, and S.C. Won, "A PWM buck-boost AC chopper solving the commutation problem," *IEEE Trans Ind. Electron.*, vol. 45, no. 5, pp. 832–835, Oct. 1998.

[9] J. P. Contreras, "Under-voltage and over-voltage AC regulator using AC/AC chopper," in *Proc. IEEE Int. Symp. Ind. Electron.*, 2006, vol. 2, pp. 809–814.

[10] N. Abd El-Latif Ahmed, K. Amei, and M. Sakui, "Improved circuit of AC choppers for single-phase systems," in *Proc. Power Convers. Conf.*, 1997, vol. 2, pp. 907–912.

[11] F. Peng, L. Chen, and F. Zhang, "Simple topologies of PWM AC-AC converters," *IEEE Power Electron. Lett.*, vol. 1, no. 1, pp. 10–13, Mar. 2003.

[12] A. Khoei and S. Yuvarajan, "Single-phase AC-AC converters using power MOSFETs," *IEEE Trans Ind. Electron.*, vol. 35, no. 3, pp. 442–443, Aug. 1988.

[13] J. Perez, V. Cardenas, L. Moran, and C Nunes, "Single-phase AC-AC converter operating as a dynamic voltage restorer," in *Proc. 32nd IEEE Annu. Conf. Ind. Electron.*, 2006, pp. 1938–1943.

[14] C.-Y. Park, J.-M. Kwon, and B.-H. Kwon, "Automatic voltage regulator based on series voltage compensation with ac chopper," *IET Power Electron.*, vol. 5, no. 6, pp. 719–725, Jul. 2012.

[15] G.-T. Kim and R.-Y. Kim, "A cost-effective AC-AC voltage sag protector with a fast dynamic response using a new RMS averaging method," in *Proc. IEEE 23rd Annu. Appl. Power Electron. Conf. Expo.*, 2008, pp. 443–448.

[16] B.-D. Min and B.-H. Kwon, "Novel PWM line conditioner with fast output voltage control," *IEE Proc. Electr. Power Appl.*, vol. 145, no. 2, pp. 85–91, Mar. 1998.

[17] O. Kiselychnyk, M. Bodson, and J. Wang, "Linearized state-space model of a self-excited induction generator suitable for the design of voltage controllers," *IEEE Trans Energy Convers.*, vol. 30, no. 4, pp. 1310–1320, Dec. 2015.

[18] B. Bahrani, A. Rufer, S. Kenzelmann, and L. A. C. Lopes, "Vector control of single-phase voltage-source converters based on fictive-axis emulation," *IEEE Trans Ind. Appl.*, vol. 47, no. 2, pp. 831–840, 2011.

[19] J. Wang, U. Kotta, and J. Ke, "Tracking control of nonlinear pneumatic actuator systems using static state feedback linearisation of input/output map," *Proc. Estonian Acad. Sci. Phys. Math.*, vol. 56, no. 1, pp. 47–66, 2007.

[20] F. E. U. Reis, R. P. Torrico-Bascope, and M. V. S. Costa, "LQR control with integral action applied to a high gain step-up DC-DC converter," in *Proc. Brazilian Power Electron. Conf.*, 2011, pp. 256–261.

[21] D. Shuai, Y. Xie, and X. Wang, "Optimal control of Buck converter by state feedback linearization," in *Proc. World Congr. Intell. Control Autom.*, 2008, pp. 2265–2270.

[22] P. C. Young and J. C. Willems, "An approach to the linear multivariable servomechanism problem," *Int. J. Control*, vol. 15, no. 5, pp. 961–979, May 1972.

Hao Liu received the B.E. degree in electrical engineering and automation from the Huazhong University of Science and Technology, Wuhan, China, and the Ph.D. degree in engineering from the University of Warwick, Coventry, U.K., in 2010 and 2015, respectively.

His main research interests include power electronics application, mathematical modeling, real time control algorithm, and hardware in the loop simulation.

Jihong Wang (M'06–SM'09) received the B.E. degree in electrical engineering from the Wuhan University of Technology, Wuhan, China, the M.Sc. degree in electrical engineering from the Shandong University of Science and Technology, Shandong, China, and the Ph.D. degree in control system theory from Coventry University, Coventry, U.K., in 1982, 1985, and 1995, respectively.

She is currently a Professor of power systems and control engineering at the School of Engineering, University of Warwick, Coventry, U.K. Her main research interests include nonlinear system control, system modeling and identification, power systems, energy-efficient systems, and applications of intelligent algorithms.

Oleh Kiselychnyk (M'15) received the M.Sc. and Ph.D. degrees in electrical engineering and automation from the National Technical University of Ukraine "Kiev Polytechnic Institute" (NTUU "KPI"), in 1993 and 1997, respectively.

He is currently an Assistant Professor in the School of Engineering, University of Warwick, Coventry, U.K. He was a Docent of the Department of Electrical Drives of NTUU "KPI." He was also a Visiting Fulbright Scholar at the University of Utah, Salt Lake City, UT, USA, in 2009, and a Visiting German Academic Exchange Service Researcher at the Hamburg University of Technology, Hamburg, Germany, in 2008. His main research interests include control of electrical motors and generators, automation of water supply systems, and microcontrollers.